Finite Element Modeling of Reinforced Concrete Beams Exposed to Fire

W. Y. Gao[1], Jian-Guo Dai[2], J. G. Teng[3] and G. M. Chen[4]

Abstract: The practical implementation of performance-based fire safety design of reinforced concrete (RC) structures hinges on the availability of accurate numerical simulation tools for the behavior of RC members exposed to fire. This paper presents a three-dimensional (3D) finite element (FE) model for the accurate prediction of both the thermal and the mechanical behavior of RC beams exposed to fire. In this FE model, particular attention is paid to the modeling of interfacial bond-slip behavior between the reinforcing steel and the concrete, an aspect which has rarely been considered by previous numerical studies. Results obtained from this FE model are compared with existing test data to examine the accuracy of the model. This comparison shows that the inclusion of the steel-to-concrete interfacial behavior leads to more accurate predictions of the deflection of RC beams exposed to fire. Predictions from this FE model also allow the complex distribution and evolution of stresses in the reinforcing steel and the concrete to be examined in detail, leading to a better understanding of the local responses of RC beams exposed to fire. The FE model presented in the paper can be used directly in performance-based fire safety design of RC beams; it can also be employed in parametric studies aimed at developing simple design rules.

Keywords: Fire resistance; Finite element model; Reinforced concrete beams; Bond-slip behavior; Steel-to-concrete interfaces; Performance-based design.

1. INTRODUCTION

Fire is one of the most severe conditions which may be encountered by a reinforced concrete (RC) building during its service life. Therefore, the fire resistance of RC members is an important issue that needs to be considered in the design of RC buildings. In current design codes, such as BS 8110-2 [1], FIP/CEB [2], ACI 216.1 [3] and AS 3600 [4], the fire resistance period of an RC member is usually determined using a prescriptive approach, such as the tabulated method which specifies some deemed-to-satisfy requirements of the minimum member dimensions and the minimum concrete cover for the reinforcing steel. These requirements are usually derived from empirical approaches and rely heavily on the limited results from fire resistance tests of RC members in which an RC member is commonly pre-loaded and exposed to a prescribed temperature-time curve as defined by BS 476-20 [5], ISO 834-1 [6] or ASTM E119 [7].

The prescriptive approach as mentioned above generally results in a conservative design, but it is not based on an accurate understanding of the thermal and mechanical behavior of RC

[1] PhD Candidate, Department of Civil and Environmental Engineering, The Hong Kong Polytechnic University, Hong Kong, China.

[2] Assistant Professor (Corresponding author), Department of Civil and Environmental Engineering, The Hong Kong Polytechnic University, Hong Kong, China, Tel: (852) 2766 6026; Fax: (852) 2334 6389; E-mail: cejgdai@polyu.edu.hk.

[3] Chair Professor of Structural Engineering, Department of Civil and Environmental Engineering, The Hong Kong Polytechnic University, Hong Kong, China.

[4] Associate Professor, School of Civil and Transportation Engineering, Guandong University of Technology, Guangzhou, China.

members exposed to fire. As a result, the prescriptive approach provides little insight into the effects of many important factors, including the geometrical configuration, load level, restraint condition, temperature-dependent material properties, cracking and tension stiffening behavior of concrete, and acceptable failure criterion of RC members exposed to fire [8,9].

Recent years have seen a gradual transition from the prescriptive approach to the performance-based approach in the fire safety design of RC members since the latter provides a more cost-effective, flexible and rational tool and allows designers to use multiple routes to achieve the required fire safety [10-13]. The performance-based fire safety design approach requires tools for the accurate fire resistance analysis of RC members (or systems), which has motivated the development of numerical simulation tools with the desired capability. Such a numerical simulation tool is generally capable of a three-step analysis: (a) fire scenario analysis, (b) heat transfer analysis, and (c) mechanical response analysis [14-16].

Many numerical models have been presented to simulate the thermal and mechanical behavior of RC beams exposed to fire. In these numerical models, the heat transfer analysis is conducted mostly using the finite difference method or the FE method [8,17-25] although empirical formulas have occasionally been used [26-28]. The mechanical response of RC beams is evaluated using either the traditional sectional analysis [8,18,21,22,24,26,27] or the FE method; in the latter case, beam elements [17-20,25,29-31] or isoparametric four-node quadrilateral elements [32] have both been employed. The focus of the existing studies has been on the reliable prediction of strength degradation, deflection or rate of deflection, which can be used as a performance index to define the fire limit state.

Exposure of an RC beam to elevated temperatures during a fire leads to significant losses in the strength and stiffness of the concrete and the reinforcing steel as well as the bond between them. However, in all existing numerical models, except the model presented in a recent publication by Huang [33], the reinforcing steel is usually assumed to be fully or perfectly bonded to the concrete at elevated temperatures. This assumption may be appropriate for predicting deteriorations in the load-carrying capacity of an RC beam exposed to fire since the critical factors are the temperature history and the deterioration in material strength. However, in performance-based fire safety design, the deflection or the rate of deflection may become a significant performance index for defining the failure limit of an RC member [22]. It is obvious that the bond-slip response of the reinforcing steel may significantly influence the deflection or the rate of deflection of an RC beam at elevated temperatures. Indeed, early pull-out tests found that the bond between steel and concrete degrades faster than the reinforcing steel itself at elevated temperatures [34, 35]. It is worth mentioning that, for an un-bonded post-tensioned RC beam exposed to fire, the bond between steel and concrete in the anchorage zones is a critical issue since sudden structural failure may occur due to the loss of anchorage bond [36].

It should also be mentioned that the tension-stiffening effect of concrete derived from the bond between reinforcing steel and concrete has been widely recognized as a fundamental mechanism that governs the deflection response of an RC member at ambient temperature; it has thus attracted extensive research attention. However, research on RC members subjected to elevated temperatures is still very limited. Recently, Pothisiri and Panedpojaman [37] analyzed the bond degradation and pull-out behavior of reinforcing steel in concrete subject to elevated temperatures by considering the effect of elevated temperature on the tension softening behavior of concrete. Huang [33] modeled both the steel-to-concrete interface and RC beams subjected to elevated temperatures and concluded that the perfect bond assumption in the analysis of RC structures exposed to fire is un-conservative, but he did not propose a bond-stress slip model for the steel-to-concrete interface at elevated temperatures.

Apart from the deflection, another important issue in the performance-based fire safety design of RC members is the localized cracking behavior of reinforced concrete and its effect

on structural integrity, which is usually ignored in the existing numerical models. Concrete cracking in RC beams exposed to fire has a number of important consequences. First, the bond behavior between steel and concrete is associated with the extent of localized damage (crack propagation) in the concrete surrounding the reinforcing steel [38-40]. Second, concrete cracking (and its effect on the bond) affects the local exposure condition of the reinforcing steel. Third, concrete cracking has a significant bearing on structural integrity and post-fire serviceability or reparability; in particular, when the beam is insulated or externally strengthened with a dissimilar layer of material on the beam surface, cracking of concrete may have a serious consequence. Indeed, it has been clearly established that debonding failure of the externally bonded strengthening layer depends strongly on the pattern and widths of cracks in the RC beam [41].

Against the above background, this paper presents a more accurate three-dimensional (3D) FE model for the thermal and mechanical analysis of RC beams exposed to fire. This 3D FE model inherits the important features of existing numerical models with respect to fire scenario analysis, heat transfer analysis and mechanical response analysis. In addition, the model includes a rigorous procedure to account for the tension-stiffening effect of concrete for accurate predictions of cracks and deflections; the latter is achieved through the accurate modeling of the bond behavior between reinforcing steel and interface. The accuracy of the FE model is demonstrated through comparisons with existing test results while its capability is illustrated through an examination of local responses predicted by the model.

2. MODELLING OF CONCRETE

2.1. General

The thermal and mechanical responses of RC beams exposed to fire depend strongly on the material properties of both concrete and reinforcing steel. Extensive studies conducted over the past few decades have led to a comprehensive understanding of the thermal and mechanical properties of concrete and steel at elevated temperatures, and this information is now widely available [9,14,42,43]. The modeling of the behavior of concrete in the present FE model is discussed in this section based on this information while that of reinforcing steel is dealt with in the next section.

2.2. Thermal Properties of Concrete

The thermal conductivity and specific heat capacity of concrete are defined according to EN 1992-1-2 [14] (Figs. 1a and 1b); the density of concrete is taken to have a constant value of 2300 kg/m^3. The effect of moisture in concrete is implicitly considered by introducing a latent heat of evaporation component to the specific heat capacity of concrete; the value of this latent heat is denoted by $C_{c,peak}$, when the temperature is between 100 ^{o}C and 115 ^{o}C, and decreases linearly when the temperature is between 115 ^{o}C and 200 ^{o}C. As shown in Fig.1b, $C_{c,peak}$ is equal to 1470 J/(kg.^{o}C) and 2020 J/(kg.^{o}C) respectively, for the moisture contents of 1.5% or 3.0% by weight. For other moisture contents, a linear interpolation is adopted.

2.3. Constitutive Model for Concrete

At elevated temperatures, the mechanical behavior of concrete is complex, involving strong nonlinearity, different failure mechanisms under compression and tension (crushing or cracking), and other temperature-dependent effects such as thermal expansion and creep. In

the present FE model, the mechanical behavior of concrete is modeled using a damaged plasticity constitutive model [44]. The key aspects of this model are summarized below.

2.3.1. Yield surface

The yield surface used in the constitutive model for concrete was initially proposed by Lubliner et al. [45] and later modified by Lee and Fenves [46] to reflect the different responses of concrete in tension and compression. The yield surface is described by:

$$F\left(\bar{\sigma},\tilde{\varepsilon}_t^{\,p},\tilde{\varepsilon}_c^{\,p}\right)=\frac{1}{1-A}\left(A\bar{I}_1+\sqrt{3\bar{J}_2}+B\left\langle\bar{\sigma}_{\max}\right\rangle-C\left\langle-\bar{\sigma}_{\max}\right\rangle\right)-\bar{\sigma}_c\left(\tilde{\varepsilon}_c^{\,p}\right) \tag{1}$$

where $\tilde{\varepsilon}_t^{\,p}$ and $\tilde{\varepsilon}_c^{\,p}$ are the equivalent tensile and compressive plastic strains, which are determined from uniaxial tension and compression tests, respectively; $\bar{I}_1$ and $\bar{J}_2$ are the first effective stress invariant and the second effective deviatoric stress invariant, respectively; $\bar{\sigma}_{\max}$ denotes the algebraic maximum eigenvalue of the effective stress tensor $\bar{\sigma}$ (Compressive stresses are defined as negative while tensile stresses are defined to be positive); $\langle\ \rangle$ is the McAuley bracket (i.e. $\langle x\rangle = x$ for $x\geq 0$ and $\langle x\rangle = 0$ for $x<0$); and A, B are dimensionless material constants and can be calculated using the following equations:

$$A=\frac{f_{bo,T}-f_{co,T}}{2f_{bo,T}-f_{co,T}} \qquad 0\leq A\leq 0.5 \tag{2}$$

$$B\left(\tilde{\varepsilon}_t^{\,p},\tilde{\varepsilon}_c^{\,p}\right)=\frac{\bar{\sigma}_{c,T}\left(\tilde{\varepsilon}_c^{\,p}\right)}{\bar{\sigma}_{t,T}\left(\tilde{\varepsilon}_t^{\,p}\right)}(1-A)-(1+A) \tag{3}$$

where $f_{bo,T}$ is the initial equibiaxial compressive yield stress at temperature T; and $f_{co,T}$ and $f_{to,T}$ are the initial uniaxial compressive and tensile yield stress at temperature T, respectively. The value of $f_{bo,T}/f_{co,T}$ increases with the temperature because the uniaxial compressive strength degrades faster than the biaxial compressive strength, causing the yield surface to exhibit a nearly elliptical shape at low temperatures but to become egg-shaped at elevated temperatures [47]. Based on experimental data, it has been proposed that the ratio $f_{bo,T}/f_{co,T}$ starts with a value of 1.16 at 20 °C and increases linearly to 1.30 at 300 °C and up to 1.70 at 750 °C [48]. $\bar{\sigma}_{c,T}\left(\tilde{\varepsilon}_c^{\,p}\right)$ and $\bar{\sigma}_{t,T}\left(\tilde{\varepsilon}_t^{\,p}\right)$ are the effective uniaxial compressive stress and effective uniaxial tensile stress respectively which can be determined from the corresponding uniaxial stress-strain relationships under compression ($\sigma_{c,T}$, ε_c) and tension ($\sigma_{t,T}$, ε_t) at temperature T:

$$\bar{\sigma}_{c,T}\left(\tilde{\varepsilon}_c^{\,p}\right)=\frac{\sigma_{c,T}}{(1-d_c)}=E_{o,T}\left(\varepsilon_c-\tilde{\varepsilon}_c^{\,p}\right) \tag{4}$$

$$\bar{\sigma}_{t,T}\left(\tilde{\varepsilon}_t^{\,p}\right)=\frac{\sigma_{t,T}}{(1-d_t)}=E_{o,T}\left(\varepsilon_t-\tilde{\varepsilon}_t^{\,p}\right) \tag{5}$$

where $E_{o,T}$ is the initial undamaged elastic modulus at temperature T; d_c and d_t are the damage variables used to define stiffness degradations in compression and tension, respectively. The definition of damage variables is important in modeling shear failures in RC beams as the shear retention factor is dependent upon the damage variables [41]. In the present study, no damage was defined as shear failure is not a critical failure mode under consideration. In biaxial compression where $\bar{\sigma}_{\max} = 0$, the surface defined above becomes the

Drucker-Prager yield function. The coefficient C is only required for triaxial compressive stress states, when $\bar{\sigma}_{\max} < 0$ and a typical value of C = 3 is recommended for normal concrete by Lubliner et al. [45].

2.3.2. Compressive behavior of concrete

The response of concrete under compression is assumed to be linear elastic until the initial yield surface is reached. The subsequent yield surfaces (i.e. loading surfaces) are controlled by a hardening variable, which is a function of the equivalent plastic strain. Therefore, based on the concept of effective stress and equivalent plastic strain, it is possible to find loading surfaces under multiaxial compression from the uniaxial compressive stress-strain relationship. In the present study, the Eurocode model [14] is adopted to define the uniaxial compressive stress-strain relationship of concrete at elevated temperatures. The compressive response of concrete is assumed to be linear elastic until the axial stress reaches the initial uniaxial yield stress which is taken to be 0.33 $f_{c,T}$ ($f_{c,T}$ denotes the uniaxial compressive strength of concrete at temperature T). This is followed by a strain-hardening curve up to the peak compressive stress and then a descending branch representing the post-peak softening behavior of concrete.

2.3.3. Tensile behavior of concrete

Before cracking, the tensile behavior of concrete is assumed to be linear elastic. The behavior of cracked concrete is simulated using an elastic-plastic constitutive model (which is a smeared crack approach) in combination with the crack band model [49]. In this smeared crack model, crack initiates when the specified yield surface (i.e. which is the same as the failure surface for tension-dominated behavior) is reached. Consequently, the tensile stress within the crack band gradually decreases while the strain increases (referred to as tension softening). In a smeared crack model, the predicted strain of cracked concrete depends on the element size [50]. In order to obtain objective (i.e. mesh-insensitive) results, a tensile stress-crack opening displacement curve rather than a tensile stress-strain curve is needed to define the softening behavior of cracked concrete. Such a tensile stress-crack opening displacement curve is defined in terms of material parameters such as the tensile strength and the fracture energy of the concrete [51]. The tensile strength $f_{t,T}$ at temperature T is taken as 0.1 $f_{c,T}$ [52]. The fracture energy G_f of concrete at ambient temperature is determined using the following equation [53]:

$$G_f = \left(0.0469\, d_a^2 - 0.5\, d_a + 26\right)\left(\frac{f_{co}}{10}\right)^{0.7} \tag{6}$$

where f_{co} is the compressive strength of concrete at ambient temperature; d_a is the maximum coarse aggregate size. For concrete beams analyzed in this study, d_a = 20 mm is assumed if this information is not reported. Very limited test results are available on the effect of elevated temperature on the fracture energy of concrete probably because the determination of fracture energy of concrete at elevated temperatures requires sophisticated measurements. Existing tests on the fracture energy of concrete at elevated temperatures were conducted using different test methods and different types of test specimens [54-59]. In addition, the loading tests in these studies were not always conducted at elevated temperatures [54,57]; that is, loading tests in some of these studies were conducted at an ambient temperature after the specimen had cooled down [55-59]. The existing test data suggest that the fracture energy of concrete does not show clear dependence on temperature (as shown in Fig.2a). In Fig. 2a, results from loading tests conducted at both elevated and ambient temperatures are included,

and the fracture energy of concrete at elevated temperatures is normalized by the value obtained at ambient temperature. Therefore, the fracture energy of concrete is assumed to be independent of temperature in the present FE model. Based on Ellobody and Bailey [52], a linearly descending branch is used in the present FE model to describe the relationship between the tensile stress and the crack opening displacement of concrete (Fig. 2b); a small residual tensile stress ($0.05\, f_{t,T}$) is assumed when $w > 0.95\, w_u$ where w is the crack opening displacement of concrete and w_u is the calculated stress-free crack opening displacement, to avoid possible difficulty in achieving numerical stability.

2.3.4. Poisson's ratio

Based on the test data of Marechal [60] and a model proposed by Elghazouli and Izzuddin [61], the Poisson's ratio of concrete is taken as 0.20 at 20 ^{o}C and to remain constant until 150 ^{o}C. Beyond the latter temperature, the Poisson's ratio is assumed to decrease linearly to 0.1 at 400 ^{o}C and to further decrease linearly down to zero at 1200 ^{o}C.

2.3.5. Decomposition of strain

The total strain of concrete at elevated temperatures includes four parts: the free thermal strain, the instantaneous stress-induced strain, the classical creep strain, and the transient creep strain [62-65], as shown in the following expression:

$$\varepsilon_{tot} = \varepsilon_{th}\left(T\right) + \varepsilon_{\sigma}\left(\overline{\sigma}, T\right) + \varepsilon_{cr}\left(\overline{\sigma}, T, t\right) + \varepsilon_{tr}\left(\overline{\sigma}, T\right) \tag{7}$$

where ε_{tot} is the total strain; t is the fire-exposure time; ε_{σ} is the stress-induced strain obtained from the above-mentioned constitutive law; ε_{th} is the free thermal strain and is determined according to EN 1992-1-2 [14]; ε_{cr} is the classical creep strain and can be ignored due to its small value compared to the other three components; and ε_{tr} is the transient creep strain which is defined as a function of stress and temperature. Transient creep appears only during the first heating cycle but not during the subsequent cooling and heating cycles [62]. It is noted that the uniaxial compressive stress-strain relationship provided by the EN 1992-1-2 [14] has implicitly incorporated the effect of transient creep as pointed out in previous studies [65,67,68]; furthermore, transient creep exists for concrete in compression rather than in tension. Therefore, the transient creep strain is not considered as a separate strain component in the present FE model. The phenomenon of concrete spalling is not considered in the present model since how it should be modeled is still controversial [69,70]. Besides, the concrete spalling has a minor effect on the fire performance of the RC beams analyzed in this study as they were made of normal strength concrete.

3. MODELLING OF STEEL

3.1. Thermal properties of steel

The temperature-dependent variations of thermal conductivity and specific heat capacity of steel as specified in EN 1993-1-2 [71] are adopted in the present FE model. The density of steel is taken to be 7800 kg/m^3.

3.2. Constitutive model for steel

The total strain of steel at elevated temperatures includes two parts: the free thermal strain ε_{th} and the stress-induced strain ε_{σ} (i.e. tensile stress-strain curve). Both are defined

in the present FE model according to EN 1992-1-2 [14].

4. MODELLING OF STEEL-TO-CONCRETE INTERFACES

Plain concrete under tension exhibits a softening post-peak response. In RC members, the tensile behavior of cracked concrete is more complicated due to bond interaction with the reinforcing steel. Although the tensile concrete located between flexural cracks does not significantly affect the load-bearing capacity of an RC beam, its ability to carry some tensile stresses after cracking does offer a stiffening effect to the steel bars. This stiffening effect is realized through the bond between the steel tension bars and the surrounding concrete and is referred to as the tension-stiffening phenomenon. Accurate modeling of this tension-stiffening effect, by accounting for slips between the steel bars and the concrete, is important in predicting the deflection of RC beams in the post-cracking range of concrete.

To model the tension-stiffening effect, various approaches have been explored. Scanlon and Murray [72] proposed the use of an average stress-strain relationship for the tensile concrete in the descending branch. Gilbert and Warner [73] proposed to modify the stress-strain relationship of the tension steel to indirectly consider the contribution of concrete on the basis of the assumption that the concrete has zero tensile resistance after cracking. These empirical approaches are able to account for the tension stiffening effect at the member level but not at the local level. A more generic approach is based on the modeling of local bond stress-slip responses of the steel-to-concrete interface using fictitious spring elements [74-77]. In a typical FE implementation of this approach, the concrete and the reinforcing steel are represented by two different sets of elements, and node pairs at the interface (i.e. at the same location) are connected using interfacial spring elements. In the present 3D FE model, three spring elements are used at each node pair: one to represent the shear bond behavior according to a bond-slip relationship and the other two to represent the normal bond behavior in the vertical directions; the latter are assumed to be rigid [78] for simplicity by assigning a large spring stiffness to the normal springs.

Limited experimental work exists on the bond behavior between reinforcing steel and concrete at elevated temperatures. The earliest pull-out test at elevated temperatures found in the published literature was conducted by Milovanov and Salmanov [79]. Their specimens were heated to several elevated temperatures and then allowed to cool down to ambient temperature before testing. In later studies, pull-out tests were conducted either at elevated temperatures [34,35,80] or at ambient temperature after cooling [80-82]. These test results suggest that the degradation of bond strength due to a temperature increase is slightly greater than that of the tensile strength of steel [34,35,81,82]. Moreover, the test results show that the degree of bond strength loss is influenced by the steel bar type (deformed or smooth), rib area and surface roughness of deformed bar, and type of aggregate. In addition, the details of the test method adopted, including the heating rate, size and shape of specimen, loading rate, and location of the reinforcing bar were also found to affect the test results. Fig.3 provides a summary of the existing pull-out test results for deformed steel bars, indicating a wide scatter; the bond strength at elevated temperature is normalized by its value at ambient temperature for clearer comparison. The diameters of the steel bars covered by Fig. 3 range from 12 mm to 20 mm while their embedded lengths range from 40 mm to 300 mm. While the bond strength generally decrease as the temperature increases, some of the test results show an opposite trend in the initial range of elevated temperatures up to around 300 ^{o}C. This unexpected increase is attributed to slightly different thermal expansion coefficients (e.g. increased confinement from the concrete to the steel) as the mechanical properties of both concrete and steel are unlikely to have changed within this temperature range. The complex scatter of the test data means difficulty in formulating an explicit equation to represent them. For the

purpose of the present study, an "upper-bound" and a "lower-bound" trend line for the normalized bond strength variation are proposed for incorporation into the FE model to reflect the effect of temperature-induced bond strength loss on the deflection of RC beams. The upper-bound line is taken to have a value of 1.25 at 300 ^{o}C and to decrease to 0.63 at 800 ^{o}C; the "lower-bound" line is taken to have a value of 0.75 at 400 ^{o}C and to decrease to 0.15 at 700 ^{o}C (Fig.3).

No information has been found in the published literature on the local bond-slip relationship of reinforcing steel at elevated temperatures. In the present FE model, the CEB-FIP bond-slip model for reinforcing steel is adopted to depict ambient temperature behavior; it is also modified for the prediction of bond-slip behavior at elevated temperatures by incorporating bond strength deteriorations as discussed above. That is, the bond-slip curve for a given elevated temperature is assumed to differ from a corresponding ambient temperature curve only in the value of the peak bond shear stress. Given the limited test data available, this assumption represents a realistic approach, and any future refinement of the bond-slip model for elevated temperatures can be easily incorporated into the FE model presented here. Based on the above considerations, the bond-slip model of reinforcing steel is given as follows:

$$\tau_{s,T} = \tau_{max,T}\left(\frac{s}{s_1}\right)^{0.4} \qquad s \le s_1 \tag{8.1}$$

$$\tau_{s,T} = \tau_{max,T} \qquad s_1 < s \le s_2 \tag{8.2}$$

$$\tau_{s,T} = \tau_{max,T} - \frac{\tau_{max,T} - \tau_{f,T}}{s_3 - s_2}\left(s - s_2\right) \qquad s_2 < s \le s_3 \tag{8.3}$$

$$\tau_{s,T} = \tau_{f,T} \qquad s > s_3 \tag{8.4}$$

where $\tau_{s,T}$ is the local bond stress at temperature T; s is the interfacial slip between reinforcing steel and concrete; s_1, s_2 and s_3 are assumed to be independent of temperature and are equal to 0.6 mm, 0.6 mm, and 1.0 mm respectively; $\tau_{max,T}$ is the peak bond stress at temperature T, which is proportional to the normalized bond strength as shown in Fig. 3; and $\tau_{f,T}$ (= $0.15\,\tau_{max,T}$) is the residual bond strength at large slips (>1.0 mm). As a result, a set of temperature-dependent bond-slip curves can be derived (Figs. 4a and 4b) for both the upper-bound and the lower-bound conditions. Following the existing studies [74-77], fictitious spring elements were used to represent the bond-slip response of the steel-to-concrete interface at elevated temperatures in the present FE model. Therefore, the tangential force transmitted via a spring element parallel to a single reinforcing steel bar is found from the following equation:

$$F_{b,T} = \pi \times D \times l_s \times \tau_{s,T} \tag{9}$$

where D is the diameter of the reinforcing bar; l_s is the average length of the two adjacent elements and $\tau_{s,T}$ is the bond stress calculated from Eqs. 8.1-8.4.

5. FINITE ELEMENT ANALYSIS

The FE software package ABAQUS [44] was used to realize the proposed FE model. The temperature-dependent bond-slip model described above was implemented into ABAQUS as a user-defined spring element. The constitutive models for concrete and steel

were defined within the framework of the software package; the modeling of RC beams exposed to fire was undertaken using the sequentially coupled thermo-mechanical procedure. In this procedure, the mechanical analysis depends on the heat transfer analysis, but no reverse dependency exists. Therefore, the FE analysis included three steps: (a) a fire scenario analysis to determine the temperature evolution of a compartment fire; (b) a heat transfer analysis of the RC beam exposed to this fire; and (c) a mechanical analysis based on the heat transfer analysis.

5.1. Fire Scenario Analysis

The temperature evolution inside a compartment fire can be evaluated by means of the two-zone fire model or computational fluid dynamics (CFD). The two-zone fire model (based on the division of a given compartment into a top hot-layer and a bottom cold-layer) has been implemented into several free programs, such as Ozone (developed at the University of Liege, Belgium [83]) and CFAST (developed at the National Institute of Standard and Technology (NIST), United States [84]). The rapid growth of computational power as well as CFD has also led to the development of CFD-based field models such as the computer program FDS (developed at NIST, United States [85]). In principle, the present FE model is capable of fire resistance analysis of RC beams exposed to any given temperature-time curve of a real compartment fire. However, since the available fire resistance tests of RC beams were conducted under the standard fire following ASTM E119 [7] or ISO 834-1 [6], the standard temperature-time relationship was employed in all the fire resistance numerical simulations presented in this paper.

5.2. Heat Transfer Analysis

To obtain the transient temperature field of an RC beam in a fire, three modes of heat transfer, namely convection, radiation and conduction should be appropriately considered. In a fire test furnace, heat fluxes flow to the outermost surfaces of the RC beam and exchange heat with them by convection and radiation, whereas heat transfer occurs within the concrete body through conduction. The time-dependent distribution of the temperature gradient in an RC beam is described by Fourier's differential equation for heat conduction [36]:

$$\frac{\partial}{\partial x}\left(k\frac{\partial T}{\partial x}\right)+\frac{\partial}{\partial y}\left(k\frac{\partial T}{\partial y}\right)+\frac{\partial}{\partial z}\left(k\frac{\partial T}{\partial z}\right)+Q=\rho c\frac{\partial T}{\partial t} \tag{10}$$

where k, ρ and c denote the temperature-dependent thermal conductivity, density and specific heat capacity, respectively; Q is the inherently generated heat; and t is the time variable. For the purpose of heat transfer analysis of an RC beam, the inherently generated heat Q is not active (i.e. $Q = 0$). The solution of the above differential equation requires the initial temperature distribution and proper boundary conditions. The initial temperature distribution in an RC beam at $t = 0$ is described by:

$$T\left(x,y,z,t\right)\Big|_{t=0}=T_0\left(x,y,z\right) \tag{11}$$

where $T_0\left(x,y,z\right)$ is the ambient temperature of the test specimen; in an actual fire test, its value is usually measured using thermocouples and the measured value varies from one test to another.

The heat fluxes exchange heat with the outermost surfaces of the RC beam via convection and radiation, which can be depicted by means of the Robin boundary conditions [36]:

$$-k\frac{\partial T}{\partial n}=h_c(T-T_f)+\sigma\varepsilon_m\varepsilon_f\left[\left(T-T_z\right)^4-\left(T_f-T_z\right)^4\right] \quad (12)$$

where n represents the outward normal direction of the beam surface; h_c is the convective heat transfer coefficient and the value is taken as 25 W/(m^2.K) [86]; T_f denotes the fire temperature measured in the furnace or determined from the standard fire curve; T_z is the absolute zero temperature; σ is the Stefan-Boltzmann constant and is equal to 5.67 × 10^{-8} W/(m^2.K^4); ε_m and ε_f are the heat emissivities of the exposed surfaces and the fire, respectively. According to EN 1991-1-2 [86], ε_f = 1.0 for the standard fire condition, and ε_m = 0.8 for concrete. For the un-exposed surfaces, a constant value of 9 W/(m^2.K) is assumed for the convective heat transfer coefficient h_c. In the FE heat transfer analysis of the present study, the concrete and the reinforcing steel were modeled using eight-node continuum (DC3D8) and two-node link (DC1D2) thermal elements, respectively.

5.3. Mechanical Response Analysis

During the mechanical response analysis, the FE mesh remained the same as that used in the preceding heat transfer analysis, but the thermal elements were replaced with stress elements, which were the eight-node continuum element with reduced integration (C3D8R) for concrete and the two-node link element (T3D2) for the reinforcing steel. The total fire exposure period was divided into small time steps. The magnitude of each time step was automatically chosen by the computer program, and the minimum time step adopted was very small (i.e. t_i = 0.2 min) to ensure numerical convergence even for a highly nonlinear problem. To investigate the convergence of the FE mesh, the beam tested by Wu et al. [87], with a section of 200 mm × 400 mm, was modeled using different meshes. Converged results for the displacement response of the beam (i.e. with a displacement tolerance of 1%) were achieved when an element size of 25 mm × 25 mm × 25 mm was used. Therefore, this element size was adopted in all the subsequent numerical simulations to strike a good balance between accuracy and efficiency.

As RC beams in fire generally experience large deflections, the effect of geometric nonlinearity was included in FE analysis using the updated Lagrangian method [44]. Similar to other studies [25,88], the Newton-Raphson method was employed as the solution method with a tolerance of 0.05 for the displacement norm as the convergence criterion. In addition, the line search function [89,90] was activated to achieve more rapid convergence.

6. VALIDATION OF THE FE MODEL

RC beams tested under fire by Wu et al. [87], Lin et al. [91] and Dotreppe and Franssen [17] respectively were selected and analyzed to illustrate the capability and accuracy of the present FE model. These tests were selected because their results have been reported in detail to facilitate FE simulations and detailed comparisons.

6.1. Tests by Wu et al. [87]

As part of a joint research project on the fire resistance of housing in China between the Fire Bureau of China and the Institute for Research in Construction of Canada, three RC beams were tested at Tianjin Fire Research Institute, China [87]. These beam specimens (Beam I, Beam II and Beam III) were designed to be identical. The dimensions and reinforcement details of these beams are shown in Fig. 5. The reinforcing steel had a yield

stress and a tensile strength of 240 MPa and 380 MPa, respectively. The measured cube compressive strength of the concrete at 28 days was 24.2 MPa. The beams were 5.1 m in span with 4.0 m of the span exposed to fire (Fig. 5). During the fire test, an overlaying slab was placed on the beam; this slab was 80 mm thick for Beams I and II but 120 mm thick for Beam III. A distributed load (i.e. 300 kg/m^2) was applied on the top of the overlaying slab, so the total load acting on the beam during the fire consisted of two parts: the applied distributed load and the self-weight of the overlaying slab.

During the heat transfer analysis, the beam was subjected to the ISO 834 standard fire from its bottom and two sides. Fig. 6a compares the predicted temperature increases at various locations in the beam with the experimental results, showing very close agreement in general. The temperature at 100 mm from the bottom face is somewhat underestimated within the first 40 minutes of fire exposure, which may be attributed to the migration of moisture toward the inner part of the beam. However, the mechanical properties of concrete and steel remain almost unchanged during this stage as the temperature is still relatively low (around 100 ^{o}C), this underestimation of temperature has little effect on the predicted fire performance of the RC beam. Figs. 6b and 6c present comparisons between the measured mid-span deflections and the FE predictions for the three beams. The three predicted curves in each figure correspond to three different assumptions for the bond behavior between steel and concrete: (a) perfect bond; (b) the upper-bound bond-slip model (Fig.4a); and (c) the lower-bound bond-slip model (Fig.4b). Clearly, the FE model provides closer predictions of deflections when the temperature-dependent local bond-slip behavior is included. The close agreement between the predictions and the test results demonstrates the validity and accuracy of the proposed FE model.

6.2. Tests by Lin et al. [91]

Another series of fire tests on RC beams were conducted at the Fire Research Laboratory of the Portland Cement Association and reported by Lin et al. [91]. A total of eleven full-scale rectangular beams were tested under the ASTM E119 standard fire. The effects of several parameters such as the aggregate type, moment redistribution and beam continuity on the fire resistance of RC beams were examined. Each beam had a total length of 9,760 mm and was installed in the fire furnace with a 6,100 mm distance between the two supports and with an 1,830 mm cantilever span beyond each support. Only one beam, named beam B-124, was simply supported during the test while all other beams were continuous at their supports, with either one or both cantilevered spans subjected to a concentred load. As the effect of beam continuity over supports is beyond the scope of this study, only beam B-124 was modelled. Beam B -124 had a section of 305 mm × 355 mm reinforced with four 19 mm steel tension bars and two 19 mm steel compression bars. The bottom and side concrete cover were 25 mm and 38 mm, respectively. The yield stress of reinforcing steel was 435.8 MPa while the cylinder compressive strength of the concrete was 29.46 MPa. The RC beam was symmetrically loaded with four concentrated loads at 1500 mm apart, and each load had a constant value of 20 kN during the test. The corner rebar temperature and mid-span deflection predicted by the proposed FE model are compared with the test data in Figs. 7, showing close agreement between the two sets of results throughout the fire exposure period. The lower-bound bond-slip model leads to more accurate predictions of the mid-span deflection whereas the perfect bond assumption leads to underestimation of the deflection, indicating that the inclusion of bond degradation at elevated temperatures leads to more accurate predictions.

6.3. Test by Dotreppe and Franssen [17]

The last test simulated was conducted by Dotreppe and Franssen [17] who reported only the fire test of one simply supported beam. The beam had a span of 6,500 mm, a width of 200 mm and a depth of 600 mm. This beam was symmetrically loaded in four-point bending with a constant moment zone of 3,150 mm. The two concentrated loads were 32.5 kN each. The bottom concrete cover was 40 mm. Comparisons between test and FE results for the temperature increase of the central tension rebar and the mid-span deflection of the beam respectively are compared in Figs. 8a and 8b. These comparisons indicate that the FE model provides consistent and satisfactory predictions of the test results throughout the entire duration of fire exposure.

6.4. Local Behavior of RC Beams Exposed to Fire

The validated FE model can be deployed to understand aspects of structural performance which cannot be easily clarified through fire tests. The local behavior of Wu et al.'s test beam, (i.e. Beams I and II) is examined herein as an example. Figs.9a-9c present the steel-concrete interfacial slip distributions for the middle tension bar along the beam span. As expected, the distribution of interfacial slips is nearly anti-symmetric with regard to the mid-span of the beam, due to the symmetry of loading and geometry of the RC beam except for the slightly different support conditions at the two ends (i.e. one end was restrained against longitudinal displacements but the other end was not), which are not expected to affect the slip distribution (Fig.5a). The maximum slip obtained with the lower-bound bond model is around twice of that obtained with the upper-bound bond model. At ambient temperature, the maximum slip always occurs near the mid-span of the beam (Fig.9a) due to the mid-span crack which is the widest among all cracks in the beam. At elevated temperatures, the maximum slip at the steel-to-concrete interface occurs unexpectedly in the transition zone between the heated and the unheated areas within the anchorage zone (Figs. 9b-9c). These results indicate that slips at elevated temperatures are mainly caused by the different thermal deformations between concrete and reinforcing steel, and these thermally-induced slips are much larger than load-induced slips at ambient temperature. In a real compartment fire, the fire exposure condition is similar to the test condition of this beam: the central part of the RC beam is exposed to fire while the parts adjacent to the beam ends are much cooler. After such fire exposure, the steel-to-concrete interface may have experienced unrecoverable slips, which may influence the residual strength and serviceability of the fire-damaged RC beam.

The variations of longitudinal distributions of stresses in the middle and the corner steel tension bars with the fire exposure time are shown in Figs. 10a and 10b. These distributions clearly indicate that all steel bars had a similar maximum tensile stress of around 50 MPa at mid-span before the fire exposure. During the fire exposure, the stresses in the tension bars increased significantly with time, and the corner bars behaved very differently from the middle bar. In the transition zone, the corner bars even developed compressive stresses, indicating that their thermal expansion was restrained by the adjacent regions (Fig. 5). When the fire exposure time exceeded about 60 minutes, the maximum stress in the middle bar experienced little further changes, whereas the maximum stress in the corner bars first increased and then decreased because of their faster deterioration due to the larger temperature increase at the corners.

Figs. 11a-11f present the predicted distributions of axial stresses in concrete over the beam cross-section at the mid-span as a function of fire exposure time obtained with the lower-bound bond model. At the beginning of fire tests (t = 0 min), the top concrete fibers are subject to compression and the bottom concrete fibers are subject to tension (Fig. 11a) as is expected. However, as the temperature increases, compressive stresses appear in the four

corner zones of the section (Fig.11b) due to the temperature gradient (i.e. U-shaped distribution) in the section. This unique stress distribution over the section causes the neutral axis to shift downward and also results in the yielding of the middle steel bar (Fig.10a). These complex stress variations are due to a combined effect of thermal stresses and interaction between reinforcing steel and concrete through interfacial bond.

Even though the spalling of concrete has not been considered in the present FE model, the predicted stress distributions shown in Fig.11 provide a good qualitative explanation for the spalling phenomenon observed in fire tests of high strength concrete (HSC) beams. Existing explanations of concrete spalling can be classified into two categories: (a) thermal stress-induced spalling (compressive stress); and (b) spalling due to the build-up of pore pressure within concrete [92]. Moreover, previous tests showed that concrete spalling occurs during the first 20-60 minutes in a fire [93]. As shown in Fig. 11f, the spalling zones observed in the fire tests of HSC beams [94,95] are almost identical to the compressive stress zones predicted by the FE model (Figs. 11b and 11c). This consistency demonstrates that the predicted stresses can be used for predicting concrete spalling. Therefore, the present FE analysis, due to its three-dimensional nature, has good potential for extension into a realistic predictive model for concrete spalling and for achieving improved fire-resistance analysis of HSC beams exposed to fire.

To further understand the thermal and mechanical responses of the RC beam, Figs. 12-13 show the predicted evolutions with time of temperatures, axial strains and axial stresses of concrete over two vertical paths of the mid-span beam section: one is along the integration points of the central layer of elements (Fig. 12) (i.e. near the mid-width of the beam section) and the other is along the integration points of the exterior layer of elements (Fig. 13) (i.e. near the beam side). In the FE model, the element size was 25 mm, leading to 8 elements across the beam width. As the integration point is at the centre of the element, the temperature of the integration point is taken as the average temperature of the eight nodes of the element.

As expected, before fire exposure, the axial stresses of concrete at mid-span vary linearly in the compressive zone. This is consistent with the plane section assumption. Nonlinear tension-softening is observed for the cracked concrete below the neutral axis of the mid-span section (Figs. 12d and 13d). After the commencement of fire exposure, the temperature-induced thermal strain and thus the total strain varies in a nonlinear manner down the beam height (Figs. 12b-12c and 13b-13c). As a result, the stress distribution over the beam depth also becomes nonlinear. The axial stresses of the central layer elements generally decrease with the fire exposure time in both the tensile and compressive zones (Fig.12d) although at 106 minutes, a small zone of large compressive stresses exists near the top edge of the beam; for the exterior layer elements, the compressive zone of concrete expands with the fire exposure time while the bottom concrete changes from a tensile state into a compressive state (Fig. 13d). These stress distributions indicate that it is difficult to define a neutral axis for such a beam section exposed to fire, which also illustrates the importance of three-dimensional analysis of RC members exposed to fire. These complex stress distributions are also difficult to incorporate in a relatively simple fire resistance design approach such as the widely used sectional analysis approach.

Some abrupt fluctuations at small stresses around the zero stress line are observed down both vertical paths at different times of fire exposure (Figs. 12d and 13d). These fluctuations are difficult to explain, but may be attributed to the high nonlinearity of the problem and the numerical procedure adopted by ABAQUS. Similar stress fluctuations have also been reported by Nechnech et al. [96] for an RC slab exposed to fire.

7. CONCLUSIONS

This paper has presented a 3D FE model for predicting the behavior of RC beams exposed to fire. In the proposed FE model, the bond-slip response of the interface between reinforcing steel and concrete at elevated temperatures is explicitly considered to enable more accurate predictions of deflections. The FE predictions of both the thermal and mechanical responses of RC beams have been found to be in close agreement with existing test results. These comparisons have also clarified for the first time that while the inclusion of this interfacial behavior in the FE model leads to more accurate predictions, the effect is often rather limited and may be ignored when the objective of the analysis is to obtain the global response of an RC beam. However, the 3D FE model allows an in-depth examination of the local behavior of RC beams exposed to fire in terms of stress and deformation states in both the concrete and the steel as well as their complex interaction. The proposed 3D FE model may be used directly in performance-based fire safety design of RC beams as a cost-effective numerical tool; it may also be employed in parametric studies to develop simple design rules.

A key element of the proposed FE model is the temperature-dependent bond-slip model for the reinforcing steel. In the present FE model, a lower-bound and an upper-bound bond model was proposed for use in the FE model based on the limited test results available. More work is needed to define the bond-slip relationship more accurately so that the local behavior of an RC beam exposed to fire can be more accurately predicted; the predicted global response of the beam benefits little from a more accurate bond-slip model for the steel-to-concrete interface.

ACKNOWLEDGMENTS

The authors are grateful for the financial support received from the National Basic Research Program of China (i.e. the 973 Program) (Project No.: 2012CB026201), the Construction Industry Institute (Hong Kong) /PolyU Innovation Fund (Project No: 5-ZJE8) and The Hong Kong Polytechnic University through a PhD studentship awarded to the first author.

REFERENCES

[1] BS 8110-2. Structural use of concrete. Part 2: code of practice for special circumstance. Milton Keynes: British Standards Institute; 1985.

[2] FIP/CEB. FIP/CEB Report on methods of assessment of the fire resistance of concrete structural members. Slough: Cement and Concrete Association; 2004.

[3] ACI 216.1. Code requirements for determining fire resistance of concrete and masonry construction assemblies. Detroit: American Concrete Institute; 2007.

[4] AS 3600. Concrete structures. Sydney: Standards Association of Australia, 2009.

[5] BS 476-20. Fire tests on building materials and structures. Part 20: methods for determination of the fire resistance of elements of construction (general principles). Milton Keynes: British Standards Institute; 1987.

[6] ISO 834-1. Fire resistance tests --- elements of building construction. Part 1: general requirement. Geneva: International Organization for Standardization; 1999.

[7] ASTM E119. Standard test methods for fire test of building construction and materials. Pennsylvania: American Society for Testing and Materials; 2008.

[8] Kodur VR, and Dwaikat MB. Performance-based fire safety design of reinforced concrete beams. J Fire Prot Eng 2007; 17(4): 293-320.

[9] Kodur VR, Dwaikat MS, Dwaikat MB. High-temperature properties of concrete for fire resistance modelling of structures. ACI Mater J 2008; 105(5): 517-27.

[10] Grosshandler W. Fire resistance determination and performance prediction research needs workshop: proceedings. NISTIR 6890, Gaithersburg: National Institute of Standards and Technology (USA); 2002.

[11] The Institution of Structural Engineers. Introduction to the fire safety engineering of structures. London: Institution of Structural Engineers; 2003.

[12] The Institution of Structural Engineers. Guide to the Advanced Fire Safety Engineering of Structures. London: Institution Of Structural Engineers; 2007.

[13] Beyler C, Beitel J, Iwankiw N, Lattimer B. Fire resistance testing for performance-based fire design of buildings. NIST GCR 07-971, Gaithersburg: National Institute of Standards and Technology (USA); 2007.

[14] EN 1992-1-2. Eurocode 2: design of concrete structures. Part 1-2: general rules --- structural fire design. Brussels (Belgium): European Committee for Standardization; 2004.

[15] Bailey C. Structural fire design: core or specialist subject? Struct Eng 2004; 82(9): 32-38.

[16] Bailey C. Science and technology developments in structural fire engineering. Struct Eng Int 2009; 19(2): 155-164.

[17] Dotreppe JC, Franssen JM. The use of numerical models for the fire analysis of reinforced concrete and composite structures. Eng Anal 1985; 2(2): 67-74.

[18] Ellingwood B, Lin TD. Flexural and shear behaviour of concrete beams during fires. J Struct Eng-ASCE 1991; 117(2): 440-58.

[19] Bratina S, Planinc I, Saje M, Goran T. Non-linear fire-resistance analysis of reinforced concrete beams. Struct Eng Mech 2003; 16(6): 695-712.

[20] Bratina S, Saje M, Planinc I, Saje M. The effects of different strain contributions on the response of RC beams in fire. Eng Struct 2007; 29(3): 418-30.

[21] Capua DD, Mari AR. Nonlinear analysis of reinforced concrete cross-sections exposed to fire. Fire Saf J 2007; 42(2): 139-49.

[22] Kodur VR, Dwaikat MB. A numerical model for predicting the fire resistance of reinforced concrete beams. Cem Concr Compos 2008; 30(5): 431-43.

[23] EI-Fitiany SF, Youssef MA. Assessing the flexural and axial behaviour of reinforced concrete members at elevated temperatures using sectional analysis. Fire Saf J 2009; 44(5): 691-703.

[24] Kodur VR, Dwaikat MS, Raut N. Macroscopic FE model for tracing the fire response of reinforced concrete structures. Eng Struct 2009; 31(10): 2368-79.

[25] Wu B, Lu JZ. A numerical study of the behaviour of restrained RC beams at elevated temperatures. Fire Saf J 2009; 44(4): 522-31.

[26] Purkiss JA, Claridge SL, Durkin PS. Calibration of simple methods of calculating the fire safety of flexural reinforced concrete members. Fire Saf J 1989; 15(3): 245-63.

[27] Desai SB. Design of reinforced concrete beams under fire exposure conditions. Mag Concr Res 1998; 50(1): 75-83.

[28] Eamon CD, Jensen E. Reliability analysis of prestressed concrete beams exposed to fire. Eng Struct 2012; 43: 69-77.

[29] Pulmano AV, Shin SY. Simplified finite-element analysis of deflections of reinforced concrete beams. ACI Struct J 1987; 84(4): 342-48.

[30] Riva P, Franssen JM. Non-linear and plastic analysis of RC beams subjected to fire. Struct Concr 2008; 9(1): 30-43.

[31] Huang ZH, Burgess IW, Plank RJ. Three-dimensional analysis of reinforced concrete beam-column structures in fire. J Struct Eng-ASCE 2009; 135(10): 1201-12.

[32] Huang ZH, Platten A. Nonlinear finite element analysis of planar reinforced concrete members subjected to fires. ACI Struct J 1997; 94(3): 272-82.

[33] Huang ZH. Modelling the bond between concrete and reinforcing steel in a fire. Eng Struct 2010; 32(11): 3660-69.

[34] Diederichs U, Schneider U. Bond strength at high temperature. Mag Concr Res 1981; 33(115): 75-84.

[35] Morley PD, Royles R. Response of the bond in reinforced concrete to high temperature. Mag Concr Res 1983; 35(123): 67-74.

[36] Purkiss JA. Fire safety engineering design of structures. 2nd ed. Butterworth-Heineman: Oxford; 2007.

[37] Pothisiri T, Panedpojaman P. Modeling of bonding between steel rebar and concrete at elevated temperatures. Constr Build Mater 2012, 27(1): 130-40.

[38] Rots JG. Bond-slip simulation using smeared cracks and/or interface element. Research Report 85.01, Structural Mechanics Group, Department of Civil Engineering, The Netherlands: Delft University of Technology; 1985.

[39] fib. Bond of reinforcement in concrete: state-of-the art report, fib Bulletin 10, Lausanne, Switzerland; 2000.

[40] Cervenka V, Cervenka J, Jendele L. Bond in finite element modelling of reinforced concrete. In: Proceeding of the EURO-C conference 2003: computational modeling of concrete structures, St Johann im Pongau, Austria; 2003. p. 189-94.

[41] Chen GM, Teng JG, Chen JF. Finite−element modeling of intermediate crack debonding in FRP-plated RC beams. J Compos Constr-ASCE 2011; 15(3): 339-53.

[42] ASCE. Structural fire protection. Manuals and reports on engineering practice No. 78, ASCE Committee on Fire Protection, Structural Division, New York: American Society of Civil Engineers; 1992.

[43] Youssef MA, Moftah M. General stress-strain relationship for concrete at elevated temperatures. Eng Struct 2007; 29(10): 2618-34.

[44] ABAQUS. ABAQUS standard user's manual, Volumes I-III, Version 6.8. Pawtucket (America): Hibbitt, Karlsson & Sorensen, Inc.; 2008.

[45] Lubliner J, Oliver J, Oller S, Onate E. A plastic-damage model for concrete. Int J Solids Struct 1989; 25(3): 299-326.

[46] Lee J, Fenves G. Plastic damage model for cyclic loading of concrete structures. J Eng Mech-ASCE 1998; 124(8): 892-900.

[47] Khennane A, Baker G. Plasticity models for the biaxial behaviour of concrete at elevated temperatures, Part I: failure criterion. Comput Methods Appl Mech Eng 1992; 100(2): 207-23.

[48] Kordina K, Ehm C, Schneider U. Effect of biaxial loading on the high temperature behaviour of concrete. In: Proceeding of the first international symposium on fire safety science, Gaithersburg, MD; 1985. p. 281-90.

[49] Bazant PZ, Oh BH. Crack band theory for fracture of concrete. Mater Struct 1983; 16(3): 155-77.

[50] Bazant PZ, Planas J. Fracture and size effect in concrete and other quasibrittle materials. Boca Raton (America): CRC press; 1998.

[51] Hillerborg A, Modeer M, Petersson PE. Analysis of crack formation and crack growth in concrete by

means of fracture mechanics and finite elements. Cem Concr Res 1976; 6(6): 773-82.

[52] Ellobody EM, Bailey CG. Modelling of unbonded post-tensioned concrete slabs under fire conditions. Fire Saf J 2009; 44(2): 159-67.

[53] CEB-FIP. CEB-FIP Model Code 90. London: Thomas Telford Ltd.; 1993.

[54] Bazant PZ, Prat CP. Effect of temperature and humidity on fracture energy of concrete. ACI Mater J 1985; 85(4): 262-71.

[55] Baker G. The effect of exposure to elevated temperatures on the fracture energy of plain concrete. Mater Struct 1996; 29(19): 383-88.

[56] Zhang B, Bicanic N. Residual fracture properties of normal- and high-strength concrete subject to elevated temperatures. Mag Concr Res 2000; 52(2): 123-36.

[57] Zhang B, Bicanic N. Fracture energy of high-performance concrete at high temperature up to 450 ^{o}C: the effects of heating temperatures and testing conditions (hot and cold). Mag Concr Res 2006; 58(5): 277-88.

[58] Nielsen CV, Bicanic N. Residual fracture energy of high-performance and normal concrete subjected to high temperatures. Mater Struct 2003; 36(262): 515-21.

[59] Tang WC, Lo TY. Mechanical and fracture properties of normal and high strength concretes with fly ash after exposure to high temperatures. Mag Concr Res 2009; 61(5): 323-30.

[60] Marechal JC. Variations of the modulus of elasticity and Poisson's ratio with temperature. In: Concrete for Nuclear Reactors. Detroit (MI): American Concrete Institute; 1972. p. 495-503 [Special publication]. SP-34.

[61] Elghazouli AY, Izzuddin BA. Analytical assessment of the structural performance of composite floors subject to compartment fires. Fire Saf J 2001; 36(8): 769-93.

[62] Khoury GA, Grainger BN, Sullivan PE. Transient thermal strain of concrete: literature review, conditions within specimens and behaviour of individual constituents. Mag Concr Res 1985; 37(132): 131-44.

[63] Schneider U. Properties of materials at high temperatures --- concrete, 2nd ed. RILEM --- Technical Committee 44-PHT, Technical University of Kassel, Kassel; 1986.

[64] Buchanan AH. Structural design for fire safety. Chichester: Wiley; 2001.

[65] Markovic M, Saje M, Planinc I, Bratina S. On strain softening in finite element analysis of RC planar frames subjected to fire. Eng Struct 2012; 45: 349-61.

[66] fib. Fire design of concrete structures --- materials, structures and modelling, fib Bulletin 38, Lausanne, Switzerland; 2007.

[67] Sadaoui A, Khennane A. Effect of transient creep on the behaviour of reinforced concrete columns in fire. Eng Struct 2009; 31(9): 2203-08.

[68] Biondini FM, Nero A. Cellular finite beam element for nonlinear analysis of concrete structures under fire. J Struct Eng-ASCE 2011; 137(5): 543-58.

[69] Pearce CJ, Kukla K, Bicanic N. Modelling of transport processes in concrete at elevated temperatures --- an alternative formulation for sorption isotherms. In: Proceeding of the EURO-C conference 2006 --- computational modelling of concrete structures, Mayrhofen, Tirol, Austria; 2006. p. 623-32.

[70] Huang ZF, Tan KH, Toh WS, Phng GH. Fire resistance of composite columns with embedded I-section steel --- effects of section size and load level. J Constr Steel Res 2008; 64(3): 312-25.

[71] EN 1993-1-2. Eurocode 3: Design of steel structures. Part 1-2: general rules --- structural fire design. Brussels (Belgium): European Committee for Standardization; 2005.

[72] Scanlon A, Murray D. Time-dependent reinforced concrete slab deflections. J Struct Div-ASCE 1974;

100(9): 1911-24.

[73] Gilbert RI, Warner RF. Tension stiffening in reinforced concrete slabs. J Struct Div-ASCE 1978; 104(12): 1885-1900.

[74] Ngo D, Scordelis AC. Finite element analysis of reinforced concrete beams. ACI J 1967; 67(3): 152-63.

[75] Schafer H. A contribution to the solution of contact problems with the aid of bond elements. Comput Methods Appl Mech Eng 1975; 6(3): 335-53.

[76] de Groot AK, Kusters GA, Monnier T. Numerical modelling of bond-slip behavior. Heron 1981; 26(1): 6-38.

[77] Ogura N, Bolander JE, Ichinose T. Analysis of bond splitting failure of deformed bars within structural concrete. Eng Struct 2008; 30(2): 428-35.

[78] Rots JG. Comparative study of crack models. In: Proceedings of the third DIANA world conference, Tokyo, Japan; 2002. p. 17-28.

[79] Milovanov AF, Salmanov GD. The influence of high temperature upon the properties of reinforcing steels and bond strength between reinforcement and concrete. Issledovanija Po Zharoupornym Betonu I Zhelezobetonu 1954; p. 203-223. in Russian.

[80] Hu KX. Researches on the bond-slip behaviour between concrete and steel bar at elevated temperatures and the fire resistance of reinforced concrete portal frames. Master thesis. Tongji University, China; 1989. in Chinese.

[81] Reichel V. How fire affects steel-to-concrete bond. Build Res Pract 1978; 6(3): 176-86.

[82] Haddad RH, Al-Saleh RJ, Al-Akhras NM. Effect of elevated temperature on bond between reinforcing steel and fiber reinforced concrete. Fire Saf J 2008; 43(6): 334-43.

[83] Cadorin JF, Franssen JM. A tool to design steel elements submitted to compartment fires---OZone V2. Part 1: pre- and post-flashover compartment fire model. Fire Saf J 2003; 38(5): 395-427.

[84] Peacock R, Jones WW, Reneke PA, Forney GP. CFAST --- Consolidated Model of Fire Frowth and Smoke Transport (Version 6). NIST Special Publication 1041, Gaithersburg: National Institute of Standards and Technology (USA); 2008.

[85] McGrattan K, McDermott R, Hostikka S, Floyd J. Fire Dynamics Simulator (Version 5). NIST Special Publication 1019-5, Gaithersburg: National Institute of Standards and Technology (USA); 2010.

[86] EN 1991-1-2. Eurocode 1: actions on structures. Part 1-2: general actions --- actions on structures exposed to fire. Brussels (Belgium): European Committee for Standardization; 2002.

[87] Wu HJ, Lie TT, Hu JY. Fire resistance of beam-slab specimens --- experimental studies. Internal Report No. 641, Institute for Research in Construction, National Research Council Canada, Canada; 1993.

[88] Rafi MM, Nadjai A, Ali F. Finite element modelling of carbon fiber-reinforced polymer reinforced concrete beams under elevated temperatures. ACI Struct J 2008; 105(6): 701-10.

[89] Crisfield MA. Accelerated solution techniques and concrete cracking. Comput Methods Appl Mech Eng 1982; 33(1-3): 585-607.

[90] Schweizerhof K. Consistent concept for line search algorithms in combination with arc-length constraints. Commun Numer Methods Eng 1993; 9(9): 773-84.

[91] Lin TD, Gustaferro AH, Abrams MS. Fire endurance of continuous reinforced concrete beams. R & D Bulletin RD 072.01B. IL(USA): Portland Cement Association; 1981.

[92] Ko J, Noguchi T, Ryu D. The spalling mechanism of high-strength concrete under fire. Mag Concr Res 2011; 63(5): 357-70.

[93] Khoury GA. Effect of fire on concrete and concrete structures. Prog Struct Eng Mater 2000; 2(4): 429-47.

[94] Choi EG, Shin YS. The structural behavior and simplified thermal analysis of normal-strength and high-strength concrete beams under fire. Eng Struct 2011; 33(4): 1123-32.

[95] Dwaikat MB, Kodur VR. Response of restrained concrete beams under design fire exposure. J Struct Eng-ASCE 2009; 135(11): 1408-17.

[96] Nechnech W, Meftah F, Reynouard JM. An elasto-plastic damage model for plain concrete subjected to high temperatures. Eng Struct 2002; 24(5): 597-611.

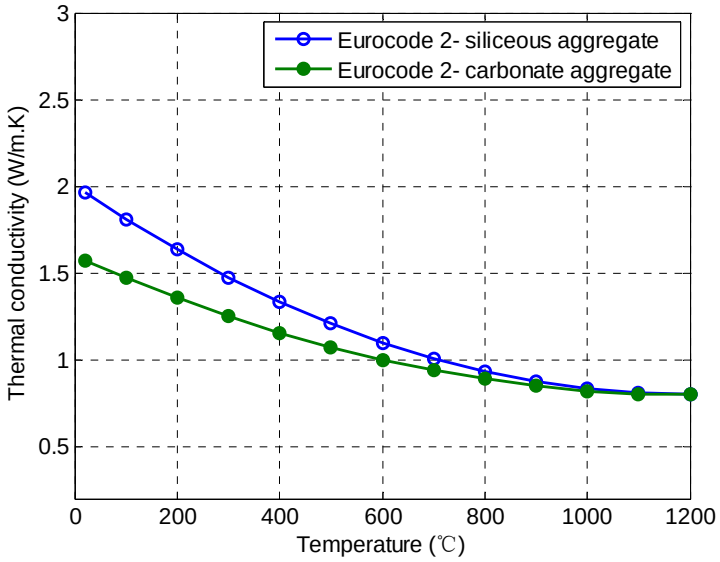

(a) Thermal conductivity

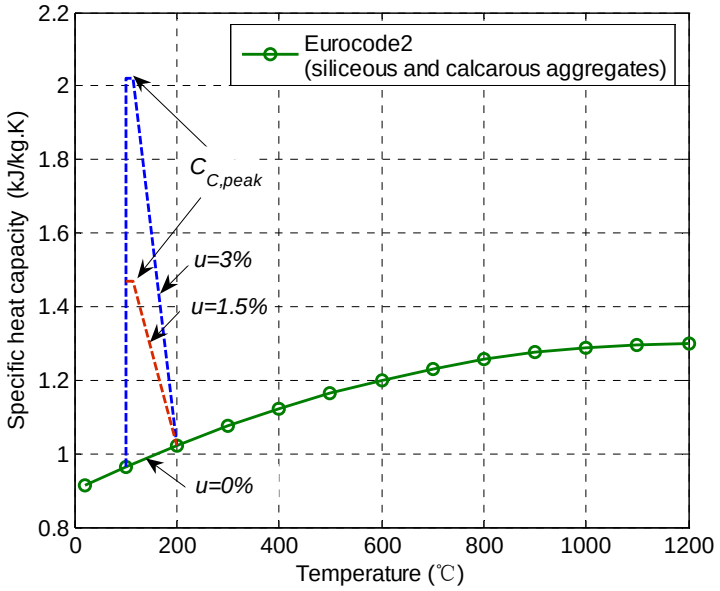

(b) Specific heat capacity

Fig. 1. Thermal properties of concrete at elevated temperatures: (a) thermal conductivity; (b) specific heat capacity.

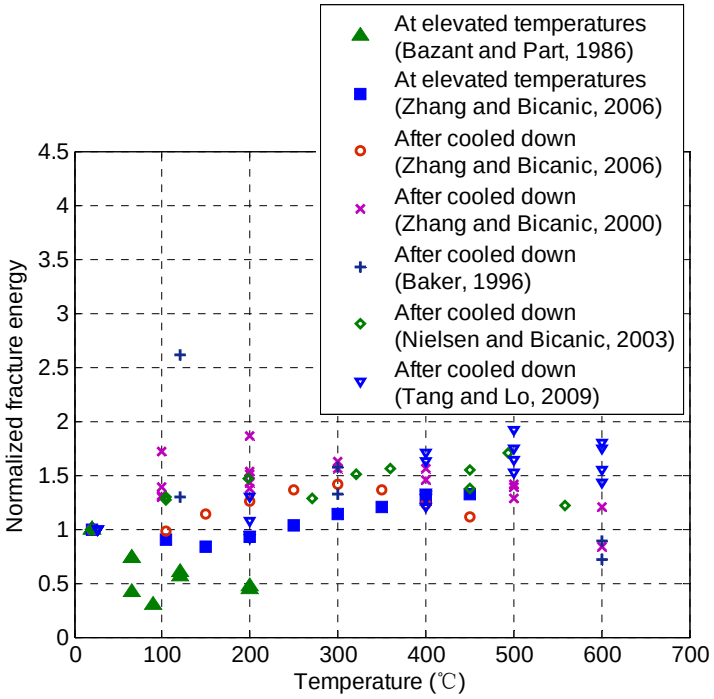

(a) Normalized fracture energy

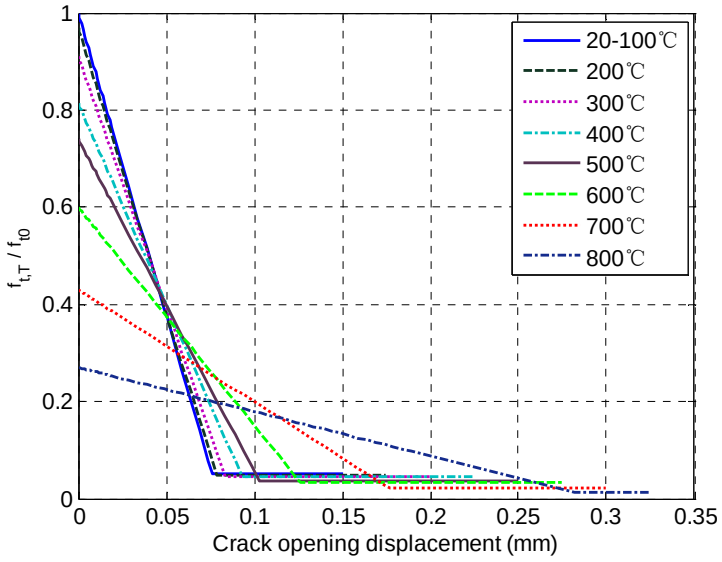

(b) Tensile stress-crack opening displacement curves

Fig. 2. Tensile behavior of concrete at elevated temperatures: (a) normalized fracture energy vs. temperature; (b) tensile stress-crack opening displacement curves

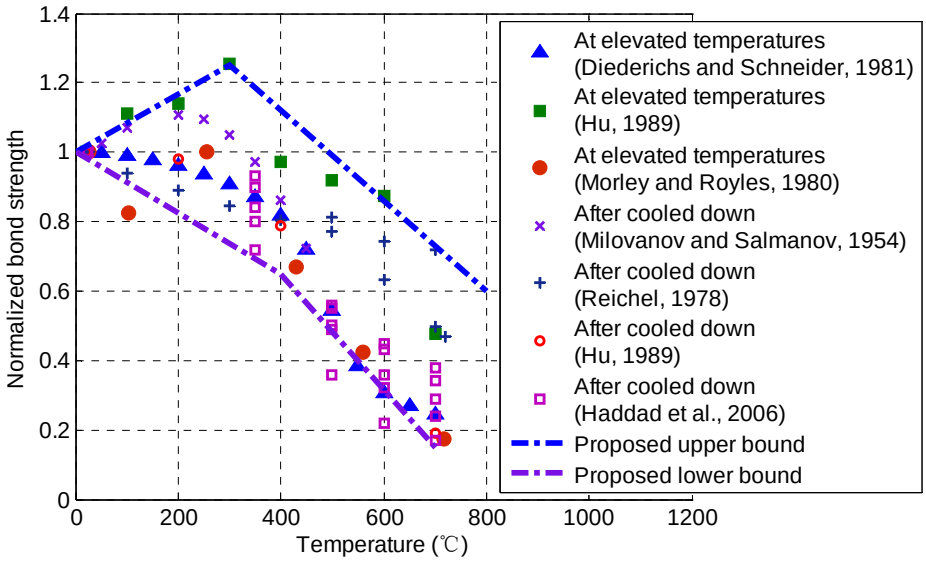

Fig. 3. Normalized bond strength and proposed upper and low bounds.

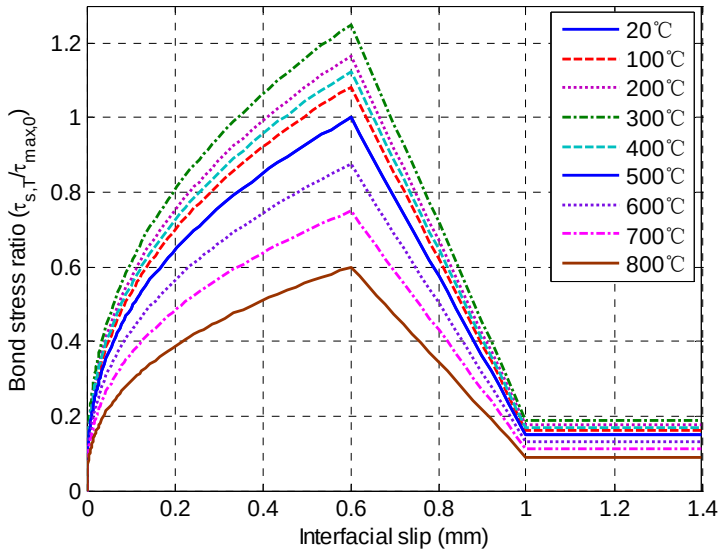

(a) Upper-bound model

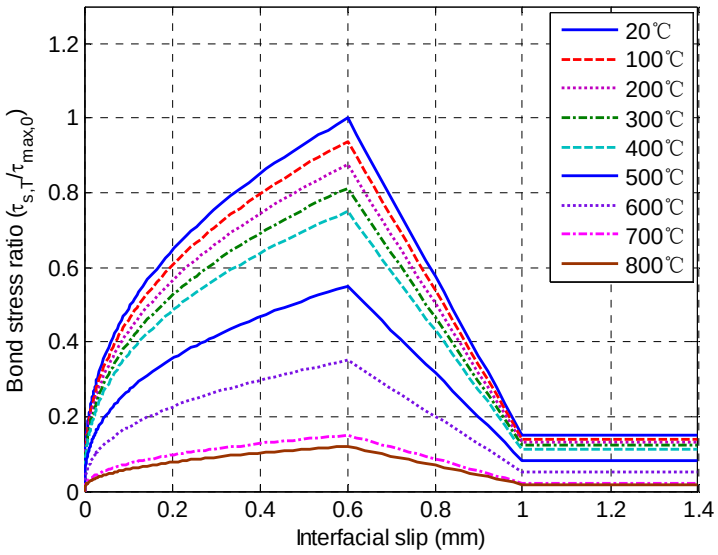

(b) Lowe-bound model

Fig. 4. Proposed local bond stress-slip curves at elevated temperatures: (a) upper-bound model; (b) lower-bound model.

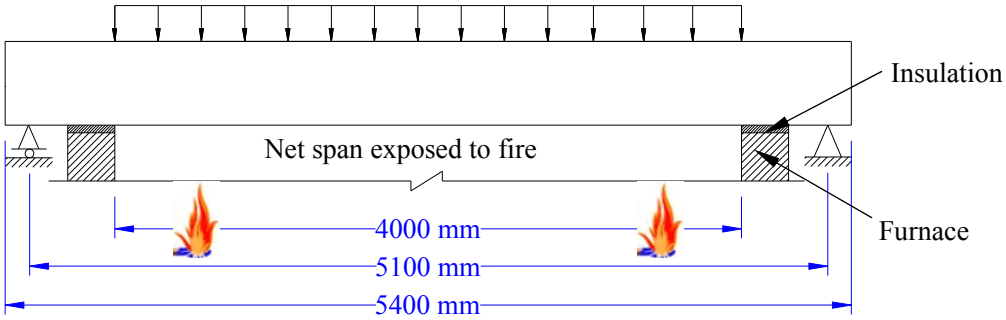

(a) Elevation

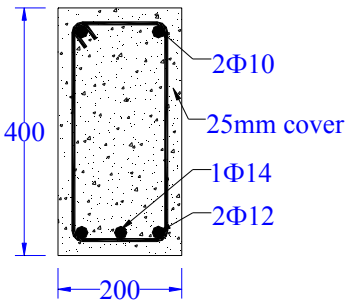

(b) Cross-section

Fig. 5. Details of specimens (200 mm × 400 mm × 5400 mm): (a) elevation; (b) cross-section.

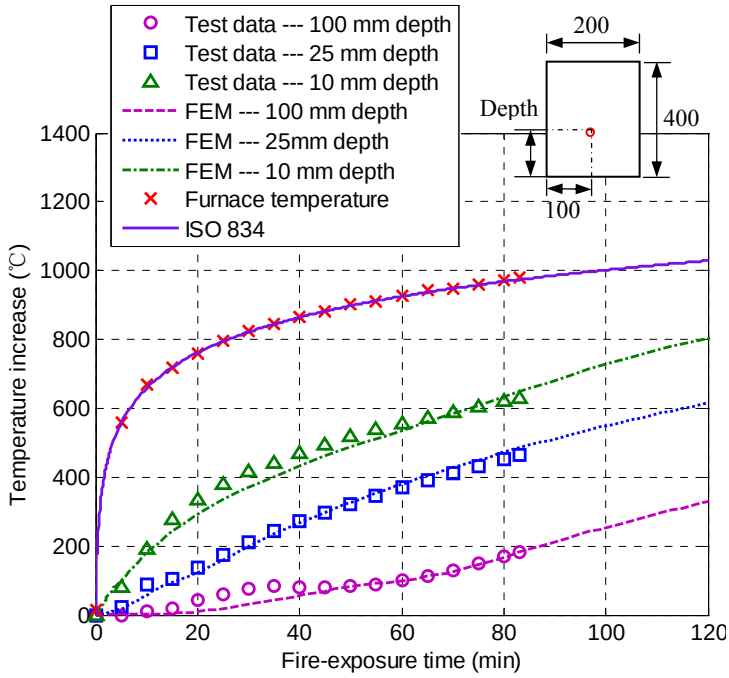

(a) Predicted and measured temperatures at various locations

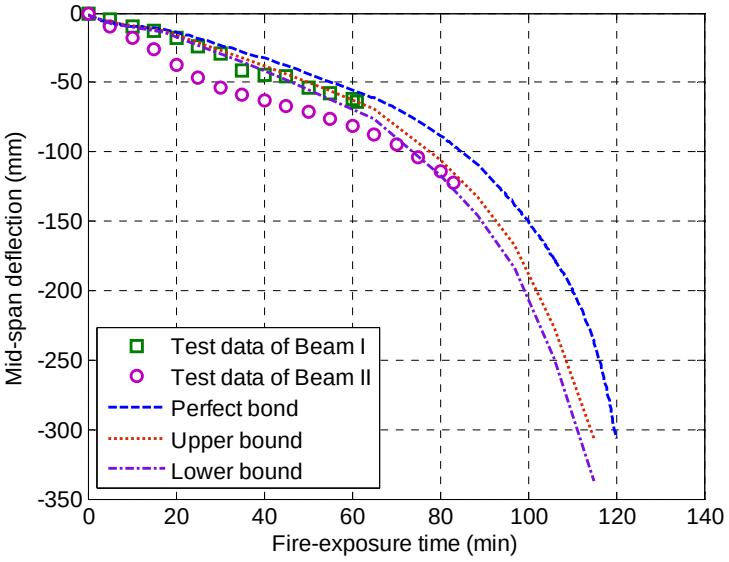

(b) Predicted and measured mid-span deflections of Beams I and II

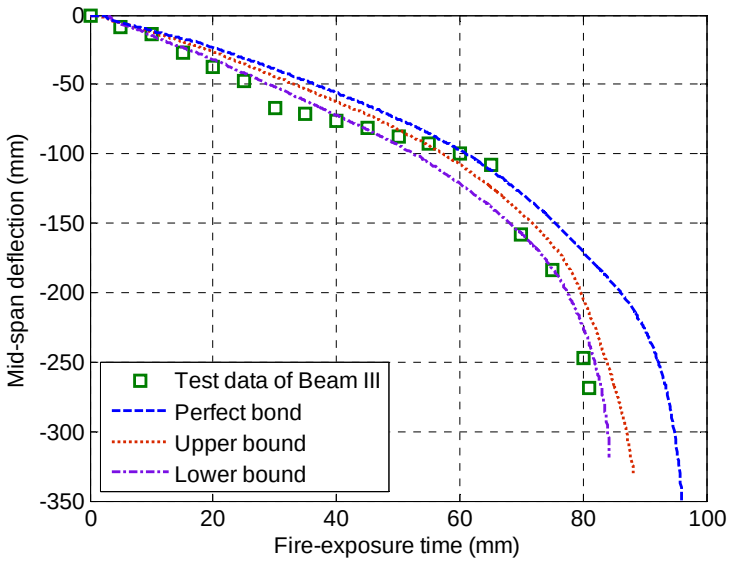

(c) Predicted and measured mid-span deflections of Beams III

Fig. 6. Comparisons of the RC beams tested by Wu et al. (1993): (a) predicted and measured temperatures at various locations; (b) predicted and measured mid-span deflections of Beams I and II; (c) predicted and measured mid-span deflections of Beams III.

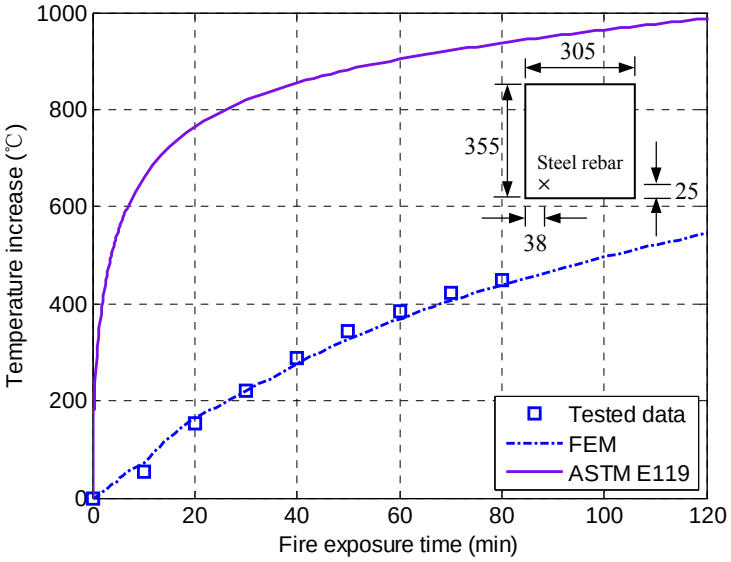

(a) Predicted and measured rebar temperatures

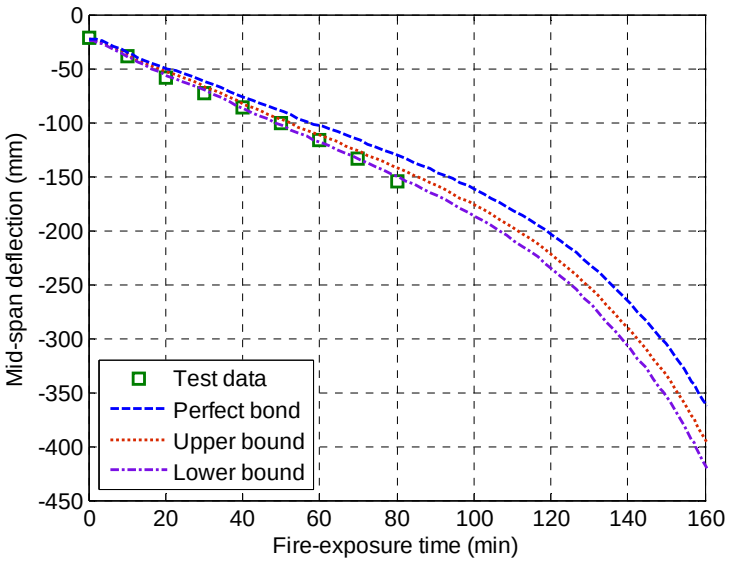

(b) Predicted and measured mid-span deflections

Fig. 7. Comparisons of the RC beam tested by Lin et al. (1981): (a) predicted and measured rebar temperatures; (b) predicted and measured mid-span deflections.

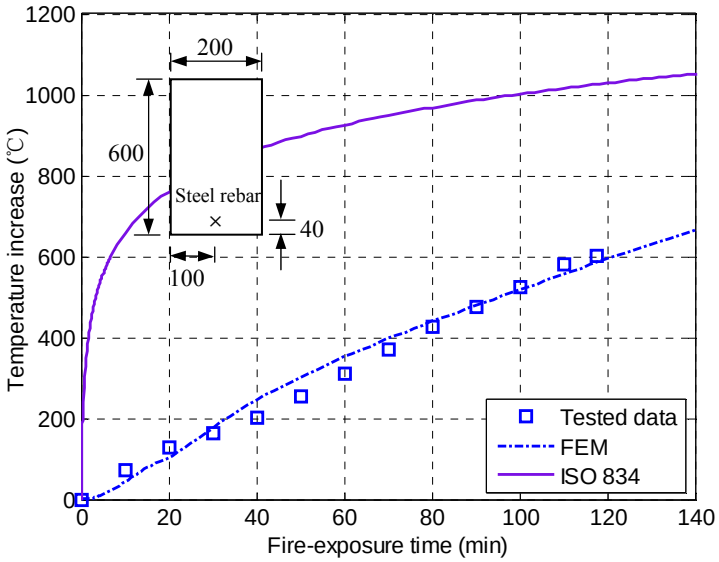

(a) Predicted and measured rebar temperatures

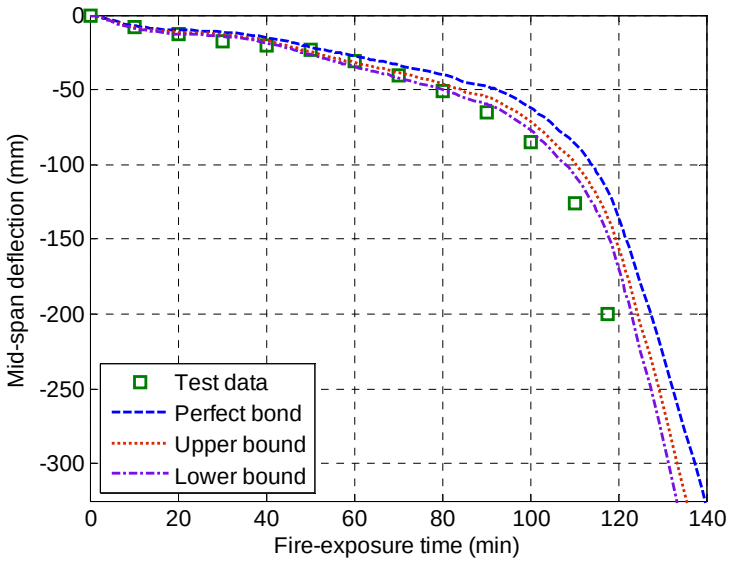

(b) Predicted and measured mid-span deflections

Fig. 8. Comparisons of the simply supported RC beam tested by Dotreppe and Franssen (1985): (a) predicted and measured rebar temperatures; (b) predicted and measured mid-span deflections.

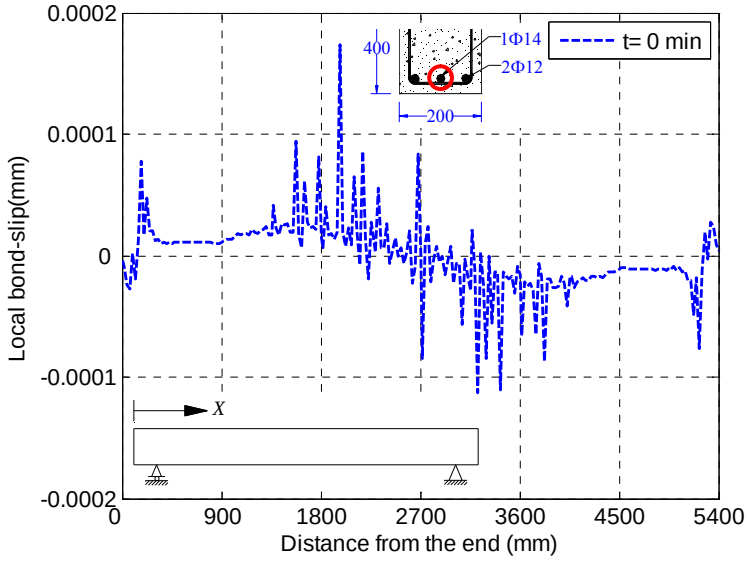

(a) t = 0 min.

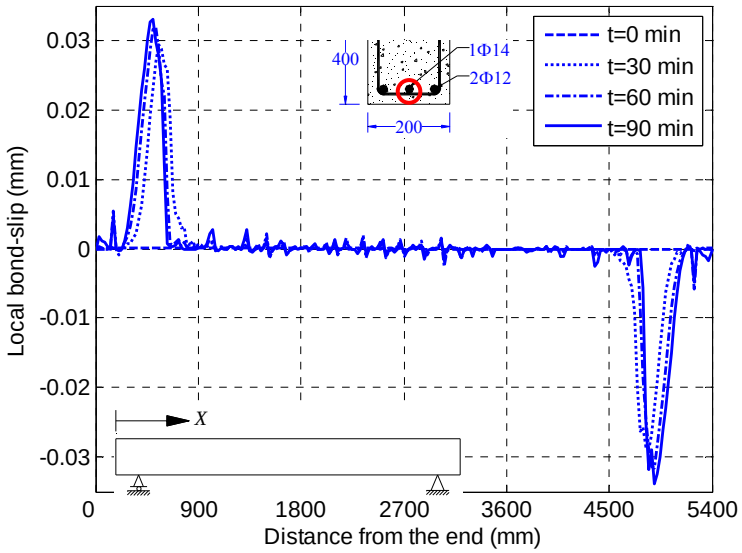

(b) t = 0, 30, 60 and 90 min with the lower-bound bond condition.

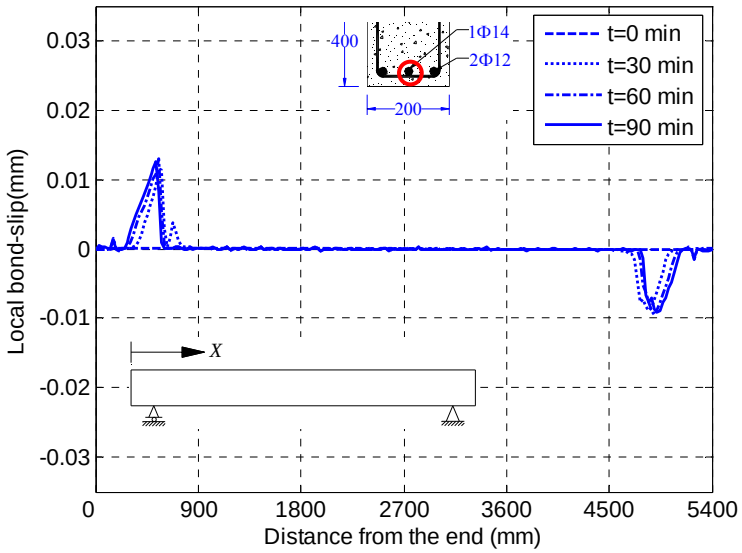

(c) t = 0, 30, 60 and 90 min with the upper-bound bond condition.

Fig. 9. Slip along the steel bar-to-concrete interface: (a) t = 0 min; (b) t = 0, 30, 60 and 90 min with the lower-bound bond condition; (c) t = 0, 30, 60 and 90 min with the upper-bound bond condition.

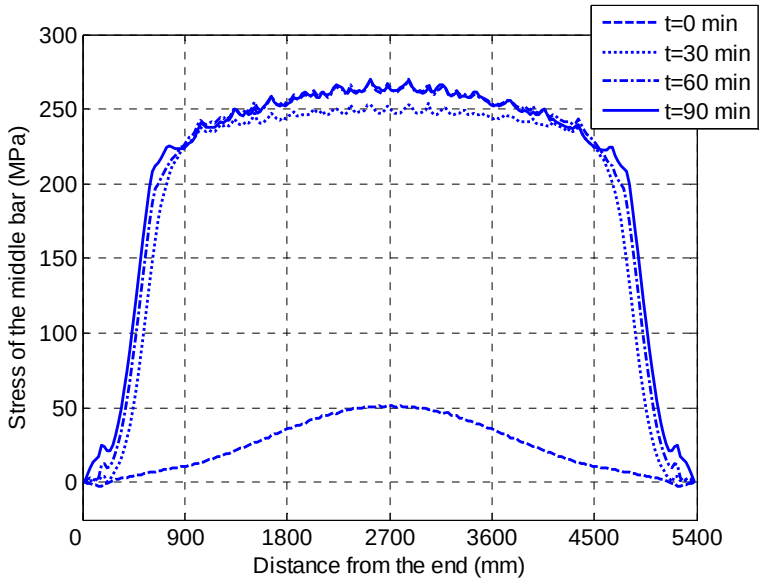

(a) Middle bar

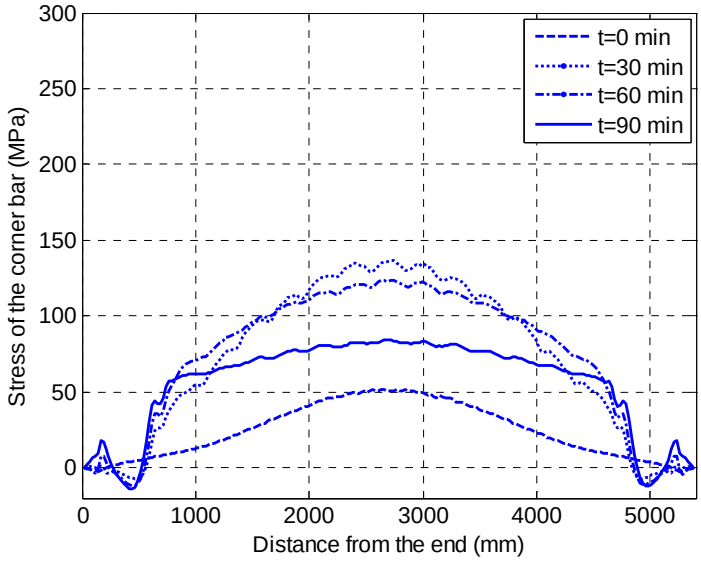

(b) Corner bar

Fig. 10. Steel stress distributions in the longitudinal direction: (a) middle bar; (b) corner bar.

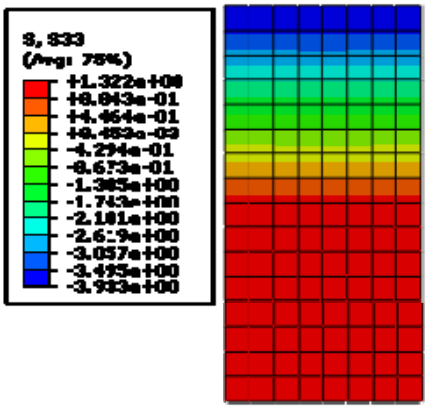

(a) t = 0 min

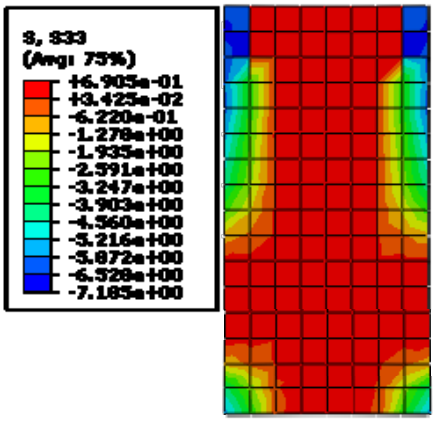

(b) t = 30 min

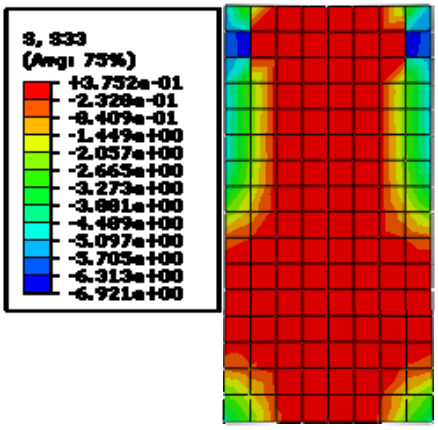

(c) t = 60 min

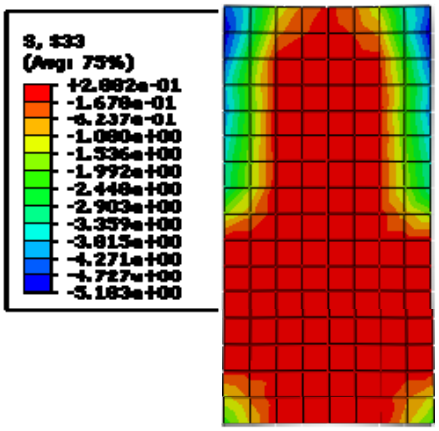

(d) t = 90 min

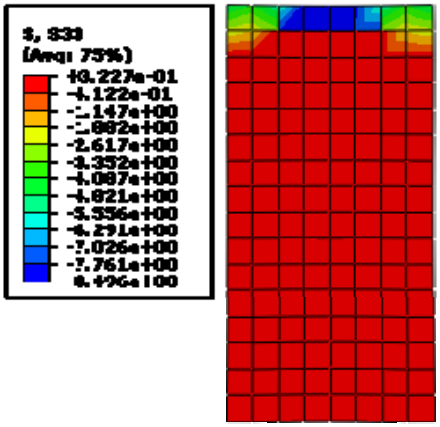

(e) t = 106 min

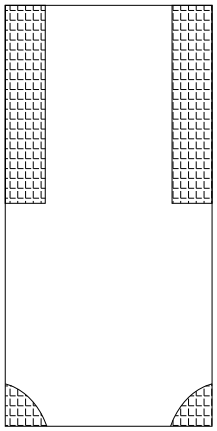

(f) Concrete spalling zones

Fig. 11. Stress distributions over the mid-span cross-section: (a) t = 0 min; (b) t = 30 min; (c) t = 60 min; (d) t = 90 min; (e) t = 106 min; (f) concrete spalling zone (Choi and Shin 2011; Dwaikat and Kodur 2009)

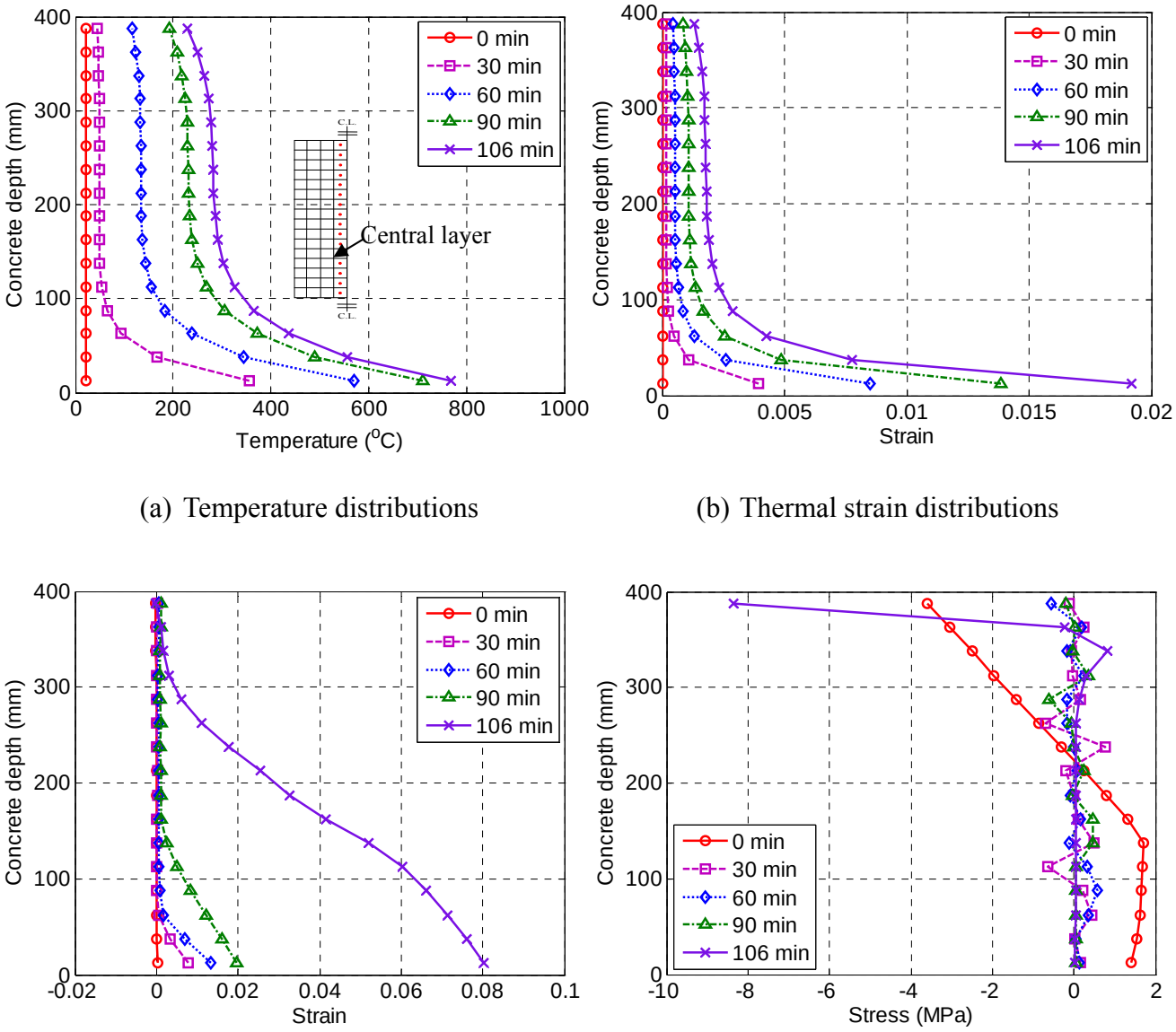

(a) Temperature distributions

(b) Thermal strain distributions

(c) Total strain distributions

(d) Stress distributions

Fig. 12. Evolutions of temperatures, strains and stresses over central layer at mid-span: (a) temperature distributions; (b) thermal strain distributions; (c) total strain distributions; (d) stress distributions.

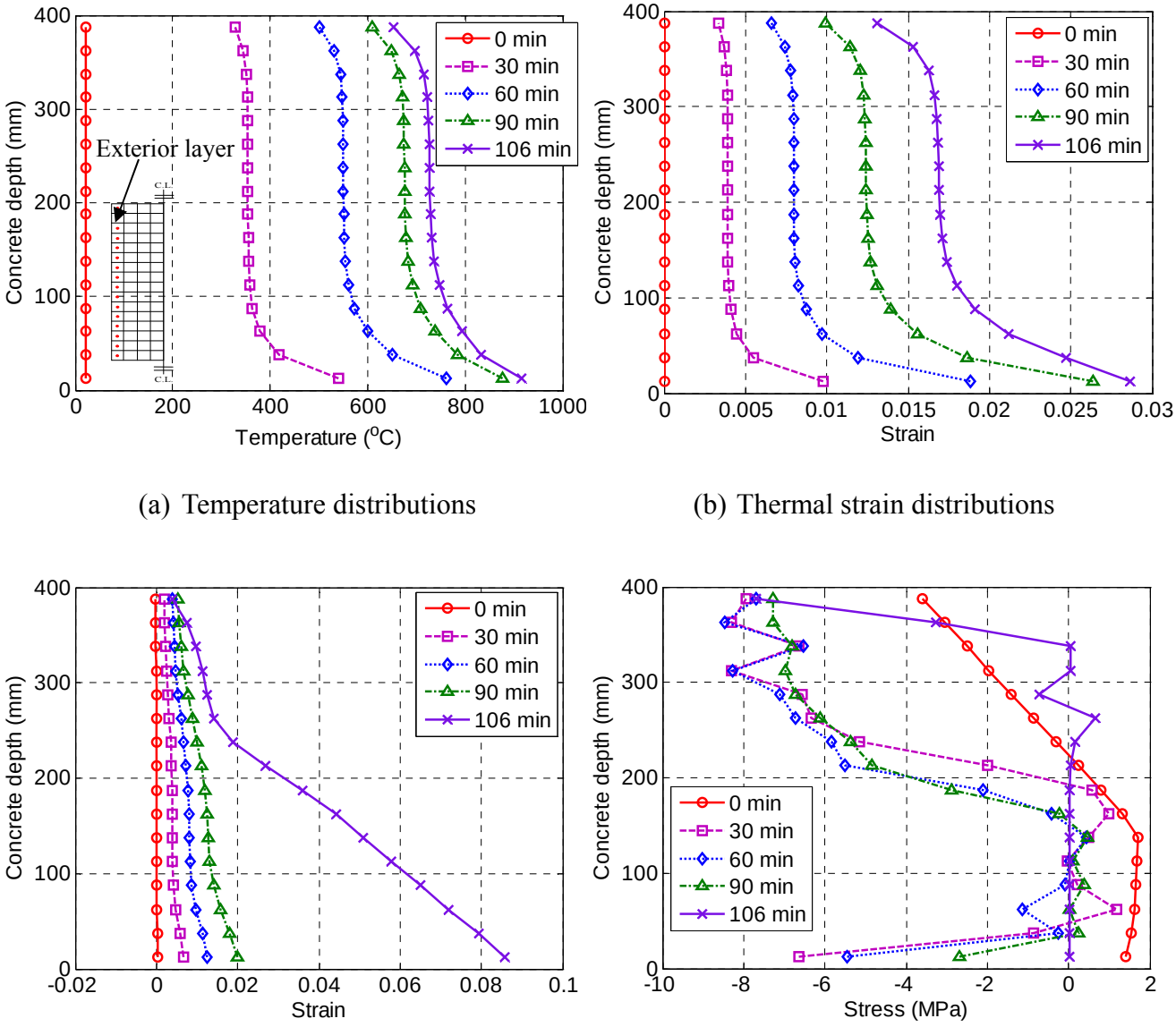

(a) Temperature distributions

(b) Thermal strain distributions

(c) Total strain distributions

(d) Stress distributions

Fig. 13. Evolutions of temperatures, strains and stresses over exterior layer at mid-span: (a) temperature distributions; (b) thermal strain distributions; (c) total strain distributions; (d) stress distributions.